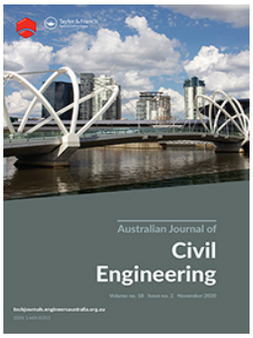

Australian Journal of Civil Engineering

ISSN: (Print) (Online) Journal homepage: https://engineersaustralia.tandfonline.com/loi/tcen20

Localised failure mechanism of concrete pedestals under bridge bearing

N. A. Yahya , M. Dhanasekar & H. Abd Hamid

To cite this article: N. A. Yahya , M. Dhanasekar & H. Abd Hamid (2020) Localised failure mechanism of concrete pedestals under bridge bearing, Australian Journal of Civil Engineering, 18:2, 164-175, DOI: 10.1080/14488353.2020.1752094

To link to this article: https://doi.org/10.1080/14488353.2020.1752094

AUSTRALIAN JOURNAL OF CIVIL ENGINEERING
2020, VOL. 18, NO. 2, 164–175
https://doi.org/10.1080/14488353.2020.1752094

Taylor & Francis
Taylor & Francis Group

ARTICLE

Localised failure mechanism of concrete pedestals under bridge bearing

N. A. Yahya [a,b], M. Dhanasekar [b] and H. Abd Hamid [a]

[a]Faculty of Civil Engineering, Universiti Teknologi MARA, Selangor, Malaysia; [b]School of Civil Engineering and Built Environment, Queensland University of Technology, Brisbane, Australia

ABSTRACT

Concrete pedestals under bridge bearing are sources of high stress zones that exhibit complex damage mechanisms under serviceability limit states. These damages are hard to detect and repair; however, if not treated early, they can lead to twisted or slant bridge girders with potential safety risks to the vehicles. With a view to understand the structural responses of these pedestals, a three-dimensional nonlinear explicit finite element modelling method has been developed and reported in this paper. The nonlinearity of the materials and the contact interaction between the bearing and the pedestal has been accounted for the model. It is shown that the model is capable of predicting the localised damages to the concrete pedestals comparable to those occur in the field. It is also shown that the sharp edges of the concrete pedestal are vulnerable to severe damages due to tensile stress singularities; modifying the shape of the edges appears prudent.

ARTICLE HISTORY
Received 7 November 2018
Accepted 1 April 2020

KEYWORDS
Bridge pedestals; localised damages; explicit finite element model; contact interface; concrete damage plasticity; stress concentration

1. Introduction

Concrete pedestals support the bridge bearings and the deck and hence can be regarded as safety critical elements in the bridge structure. These pedestals are in the critical flow path of the vertical load from the traffic and lateral loads from both traffic and other natural causes including thermal, wind and seismic actions; these loads are transferred by the pedestals to the pier crossheads. They also disperse the load from the bridge bearings to ensure split damages of the pier crossheads do not occur. The demand for bridge inspection, repairs and maintenance works due to accelerated localised damages in concrete pedestals is on the increase due to increased traffic and frequent environmental impacts. When the repaired concrete pedestals fail prematurely, the cost burden to the communities increases. Thus, the asset owners replace the old pedestals with the expectation of better performance as there exists little information on the load transfer mechanisms of concrete pedestals. Without comprehensive understanding of the load transfer mechanism and appropriate engineering design, the concrete pedestals are constructed to suit the field conditions by the construction crew. In spite of their important load transfer function, relative to bridge bearing research, only very limited research has been carried out on this area especially on high stress bearing zones of shallow concrete pedestals (Nguyen and Tassoulas 2009; Weisman and Warn 2011; Ala, Power, and Azizinamini 2016; Steelman et al. 2016; Mishra et al. 2015).

Due to lack of fundamental research, localised damages in concrete pedestals are not clearly explained and hence the maintenance is at best based on instinct rather than evidence based. Therefore, this present research aims at explaining the load transfer mechanism of concrete pedestals scientifically. Examples of localised damage of concrete pedestals include cracking of edges, edge damages and spalling of concretes as observed in several bridge inspections reported in Austroads (2012); Hite, DesRoches and Leon (2008); Freire, De Brito and Correia (2015). In the present study, the load corresponding to such localised failure modes is defined as the *localised failure load* and the load corresponding to the total collapse of concrete pedestal is defined as the *global failure load*. Figure 1 shows the schematic diagram of the localised and the global failure modes of concrete bridge pedestals.

Viljoen, Newmark and Mawman (1972) have argued that where the damage of pedestal is not mitigated in a timely manner, the progression of damages and overstressing often has led to split headstocks of piers or abutments. Bennett (2014) has criticised the load distribution methods in the Clause 12.3 of Australian standard AS5100.5 (2014) and presented examples to illustrate occurrence of high contact stresses on the concrete pedestals even when thick bearing plates are used. Localised damage due to stress concentration has also been emphasised in Zong and Dhanasekar (2013a, 2013b, 2017).

There is a large volume of published studies on the increase in compressive strength of concretes due to

CONTACT N. A. Yahya azmi_216@yahoo.com Faculty of Civil Engineering, Universiti Teknologi MARA, Selangor, Malaysia

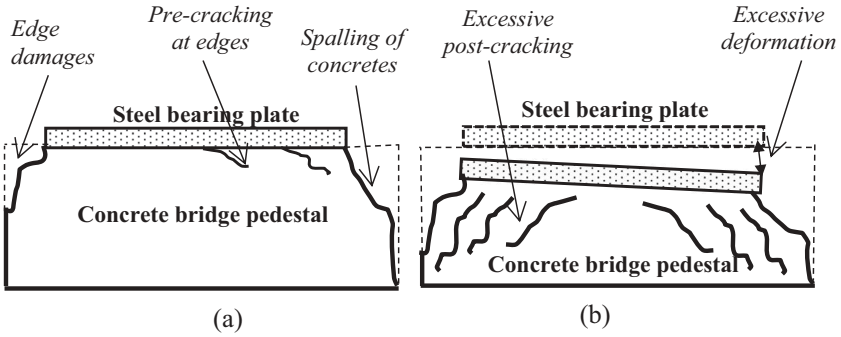

Figure 1. Schematic diagram: (a) localised failure; (b) Global failure in bridge pedestal.

confinement effects (Ince and Arici 2004; Escobar-Sandoval, Whittaker, and Dargush 2006; Roberts-Wollmann et al. 2006; Bonetti, 2014). These studies do not, however, address the contact between bearing plates and subsequent localised failure mechanisms of the confined concretes similar to those in concrete pedestals. The numerical modelling has helped developing an optimal design of complex contact surfaces by minimising the stress and damage levels especially at the contact surfaces between steel bearing plates and the concrete pedestals.

2. Brief survey of the pedestals in the field

With a view to examine the actual modes of damages in bridge pedestals, bridge engineers in the State of Queensland, Australia and Kuala Lumpur, Malaysia have been contacted. From the technical and industry reports, several images of pedestals at various stages of damage were collected. The most common failure modes, spalling of concrete and cracking of edges of the concrete pedestal, are shown in Figure 2.

It can be seen that these failures appear especially at the contact area between the steel bearing plate and the concrete pedestal surfaces. The need for careful examination of the contact interaction between the steel bearing plate and the concrete pedestal surface to explain load transfer mechanism is, thus, confirmed from this brief survey of the industry.

3. Finite element (FE) method

FE analysis was performed to predict the structural response of the concrete pedestals subjected to heavy load using ABAQUS/explicit. Explicit solver, although primarily aimed at impact load scenarios, is shown to solve static problems through appropriate mass or time scaling. Use of Explicit FE method to solve static loading was proved successful by previous studies (Genikomsou and Polak 2015; Noor-E-Khuda, Dhanasekar, and Thambiratnam 2016; Dhanasekar, Thamboo, and Nazir 2017). Generally, explicit analysis requires 10,000–1,000,000 increments to achieve converged solutions but computational cost per

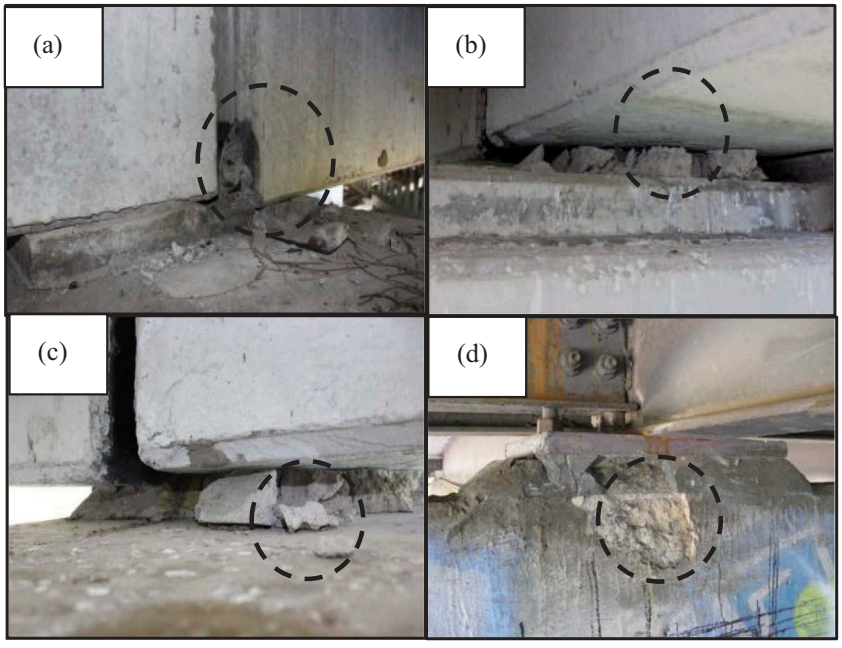

Figure 2. Common types of localised failure modes of concrete pedestals: (a) edge.

Table 1. Material input parameters for concrete strength 32MPa.

Mass density (kg/m^3) = 2400
Elastic Modulus (GPa) = 26.48
Poisson's ratio = 0.167

Ratio of initial equibiaxial compression yield stress to initial uniaxial compression yield stress $\left(\frac{\sigma_{b0}}{\sigma_{c0}}\right)$ = 1.12

Value of $\alpha = \frac{\left(\sigma_{b0}/\sigma_{c0}\right)}{2\left(\sigma_{b0}/\sigma_{c0}\right)}$ = 0.12

Value of K_c = 0.666
Value of γ = 3
Dilation angle (ψ) = 30°
Eccentricity (ϵ) = 0.1

Compression hardening		Tension stiffening	
Stress (MPa)	Crushing strain	Stress (MPa)	Cracking strain
24.02	0	2.28	0
29.21	0.0004	1.46	0.0001
31.71	0.0008	1.11	0.0003
32.36	0.0012	0.96	0.0004
31.77	0.0016	0.80	0.0005
30.38	0.0020	0.54	0.0008
28.51	0.0024	0.36	0.0010
21.91	0.0036	0.16	0.0020
14.90	0.0050	0.07	0.0030
2.95	0.0100	0.04	0.0050

increment is relatively small because no iterations required as compared to implicit analysis (Janaraj and Dhanasekar 2014). In the explicit analysis technique, dynamic equilibrium equation is used as given in Eq. 1 (Abaqus Users' Manual, 2006)

$$M\ddot{u} = P - I \tag{1}$$

$$\ddot{u}\big|_{(t)} = M^{-1}.(P - I)\big|_{(t)} \tag{2}$$

where M is the lump mass, P is the external load vector, I is the internal load vector and $\ddot{u}$ is the acceleration and t is the time.

In this method, through double integration, the displacement (u) is determined – thus, the method is more suitable for highly nonlinear problem involving contact and material nonlinearity. If the first term of this equation for inertia or dynamic force is too small, then this equation is reduced to the static equilibrium.

3.1. Concrete damage plasticity model

The concrete damaged plasticity model (CDPM) uses the concept of isotropic-damaged elasticity in combination with isotropic tensile and compressive plasticity to represent the inelastic behaviour of concrete. In contrast to the brittle cracking model, it allows the definition of strain hardening in compression (Zhara and Dhanasekar 2016ba). It is also sensitive to straining rate. The CDPM is developed based on the early work of Lubliner et al. (1989) and by Lee and Fenves (1998). Strain rate decomposition for CDPM is assumed for the rate-independent model:

$$\dot{\varepsilon} = \dot{\varepsilon}^{el} + \dot{\varepsilon}^{pl} \tag{3}$$

where $\dot{\varepsilon}$is the total strain rate, $\dot{\varepsilon}^{el}$ is the rate of change of elastic strain and $\dot{\varepsilon}^{pl}$is the rate of change of inelastic strain.

The stress–strain relations are governed by scalar damaged elasticity:

$$\bar{\sigma} = (1 - d)D_o^{el} : \left(\varepsilon - \varepsilon^{pl}\right) = D^{el} : \left(\varepsilon - \varepsilon^{pl}\right) \tag{4}$$

where D_o^{el} is the initial (undamaged) elastic stiffness of the material;$D^{el} : \left(\varepsilon - \varepsilon^{pl}\right)$ is the degraded elastic stiffness; and$d$is the scalar stiffness degradation variable in range from zero (undamaged material) to one (fully damaged material). Material input parameters of the concrete model are given in Table 1. The parameters in Table 1 referred to the typical values provided in ABAQUS (2006). Some of parameters were obtained from various publications (Jankowiak and Lodygowski 2005; Starossek, Falah, and Lohning 2010; Chaudhari and Chakrabarti 2012; Zhara and Dhanasekar 2016b). The tensile strength of concrete was determined as a function of the compressive strength of concrete, consistent with the ACI Committee 318 (1999) formula given in Eq. (5).

$$f_{ct} = 0.56\sqrt{f_{cu}} \tag{5}$$

where f_{cu} is the compressive strength of concrete cube. The tensile stress in pedestals is prescribed in AS3600 (2009) as in Eq. (6).

$$f_{ct} = 0.45\sqrt{f_c'} \tag{6}$$

In which $f_c^{'}$ is the characteristic compressive strength of concrete cylinders.

As the cube strength of concrete is larger than the cylinder strength; with a larger coefficient, it is

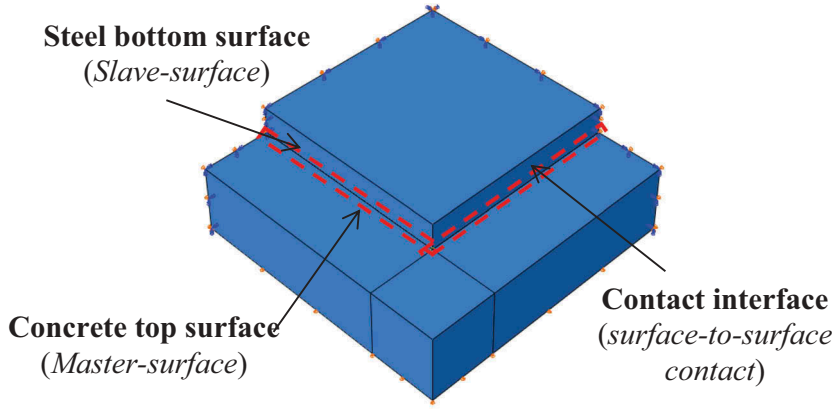

Figure 3. Contact interface of master-slave surface.

apparent that the ACI 318 (1999) allows larger tensile stress than that of the Standard (2009).

3.2. Contact interaction

The FE model consisted of the concrete pedestal and the steel bearing plate. A concrete pedestal of 400 mm length, 400 mm width and 50 mm height was considered as shown in Figure 3. The steel plate dimension was set as 300 mm length, 300 mm width and 20 mm thickness. These dimensions were set based on the estimated bearing capacity of 3500 kN consistent with Cl. 12.6, AS5100.5. A sample calculation is provided in the Appendix. By taking advantages of symmetry in both the geometrical shape and the structural loading, only quarter of the pedestal was modelled to minimise computational time.

The contact interaction due to frictional forces between the steel bearing plate surface and the concrete pedestal was represented using the hard contact definition in ABAQUS with no bonding between the bottom surface of the steel bearing plate and the top surface of the concrete pedestal. The surface-to-surface contact between steel bearing plate and the concrete bearing surface was defined using kinematic finite sliding contact algorithm where the selected master–slave surface of contact interface is shown in Figure 3.

For vertical direction, the pressure–overclosure relationship for 'hard' contact was used in order to minimise penetration of the master surface into the slave surface. For horizontal direction, tangential behaviour was assigned at the interface to represent the contact friction. In the current model, the stiffness (penalty) method was implemented with a coefficient of friction of 0.3 by Al-Rifaie et al. (2018).

In the analysis, the load effect due to lateral force such braking force or bridge curvature was not included – only vertical load was considered to simulate the permanent and the imposed loads for simply supported bridge girders.

The concrete pedestal and the steel bearing plate were modelled using 3D solid elements C3D8 R in ABAQUS (2006) as shown in Figure 4. Mesh sensitivity was analysed using five different cubic solid elements of

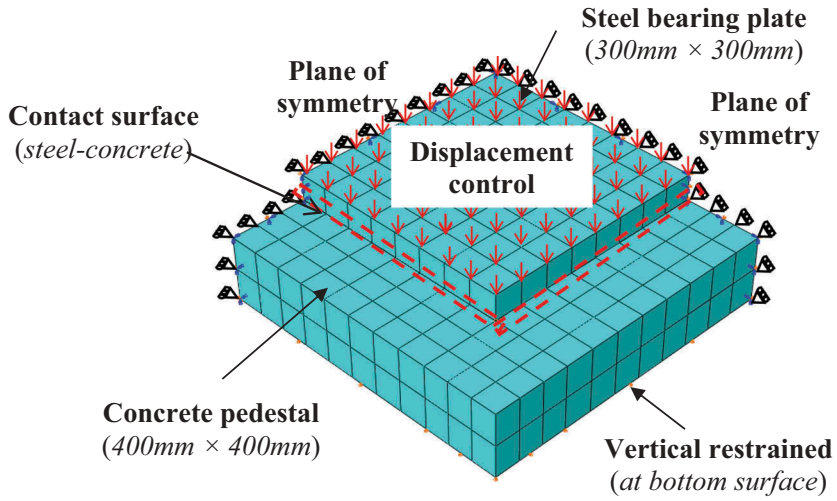

Figure 4. Meshed one-quarter model.

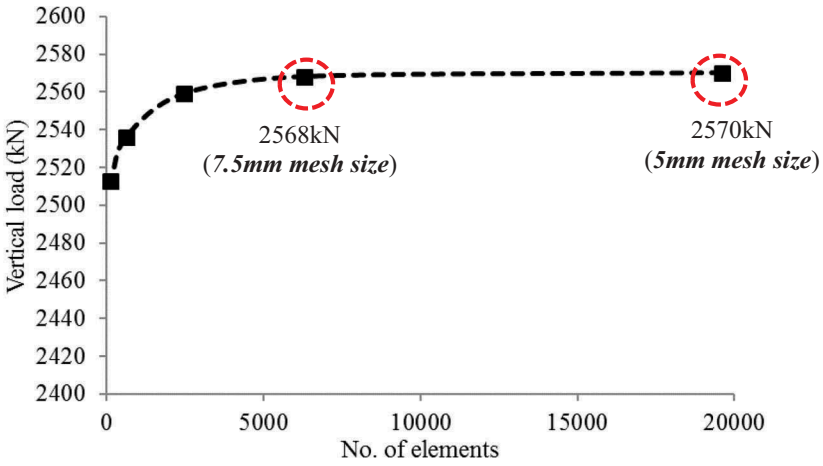

Figure 5. Different load level for different mesh sizes.

size 5, 7.5, 10, 15 and 30 mm. The response of these models for 0.2 mm compression normal to the loaded surface was used to decide the optimal mesh. Vertical load was calculated as the integral of all reaction forces at each node where the compression deformation of 0.2 mm was applied and plotted against the number of elements used in each analysis as in Figure 5. The vertical load converged when the element size was 7.5 mm.

In the analysis, vertical displacement was applied on the top surface of steel bearing plate until concrete failure occurred. The bottom surface of concrete pedestal was restrained in the vertical direction as it normally sits on the rigid bridge abutment surface. The lateral directions of the concrete edges were set free to simulate the expansion and contraction of the pedestal loading. From the FE models, analysis outputs for vertical reactions, vertical displacements, vertical stress distributions, lateral deformations and tensile stresses were examined.

3.3. Model validation

The FE model predictions were validated using the bearing capacities of concrete pedestals under different confinement effect provided by the neighbouring pier concrete at the bottom and steel bearing plates on the top. The confinement of concrete is a crucial benchmark for the validation work to ensure the FE model is capable of predicting the confinement levels for different steel plate surface areas. The ratio of contact area of the concrete surface to the steel plate surface area is a key parameter in the investigation of the confinement in the concrete pedestals. In order to examine the reliability of the FE results, a series of FE models were selected, and their results compared with the experimental work on the effects of area of concrete to area of steel plate (A_c/A_s) ratio, the shape of the bearing plate, the concrete compressive strength, the normalised confinement effect (f_b/f_{cu}) and deck sizes on the bearing strength of reinforced and plain concrete blocks conducted by Bonetti (2005). The author examined (A_c/A_s) ratios for 2, 4, 6, 8, 12 and 16; In our study, 11 concrete blocks of 406.4 mm high with different compressive strengths of 27.92, 30.06 and 31.30 MPa were used for the validation purpose as shown in Table 2.

In order to account for the differences of the compressive strengths of the tested specimens and the FE models, the experimental and the modelling results were normalised by introducing two dimensionless

Table 2. Experimental results reported by Bonetti (2006).

Concrete surface A_c (mm^2)	Steel plate surface A_c (mm^2)	A_c/A_s	Ultimate load, F_{ult} (kN)	Bearing strength, $f_b = F_{ult}/A_s$ (MPa)	Concrete Compressive strength, f_{cu} (MPa)	Confinement effect, f_b/f_{cu}
203.2	143.76 × 143.76	2	663.87	30.71	27.92	1.10
×	101.60 × 101.60	4	414.80	40.20		1.44
203.2	82.96 × 82.96	6	328.06	47.74		1.71
	71.84 × 71.84	8	289.13	56.21	30.06	1.87
	58.66 × 58.66	12	249.10	72.44		2.41
	50.80 × 50.80	16	220.19	85.37		2.84
	143.68 × 143.68	2	718.39	34.75	31.03	1.12
	128.51 × 128.51	2.5	600.51	36.31		1.17
	117.32 × 117.32	3	531.56	38.79		1.25
	101.60 × 101.60	4	465.95	45.30		1.46
	82.96 × 82.96	6	375.87	54.61		1.76

Constant height of concrete block is 406.4 mm.
Constant thickness of steel plate is 12.7 mm.

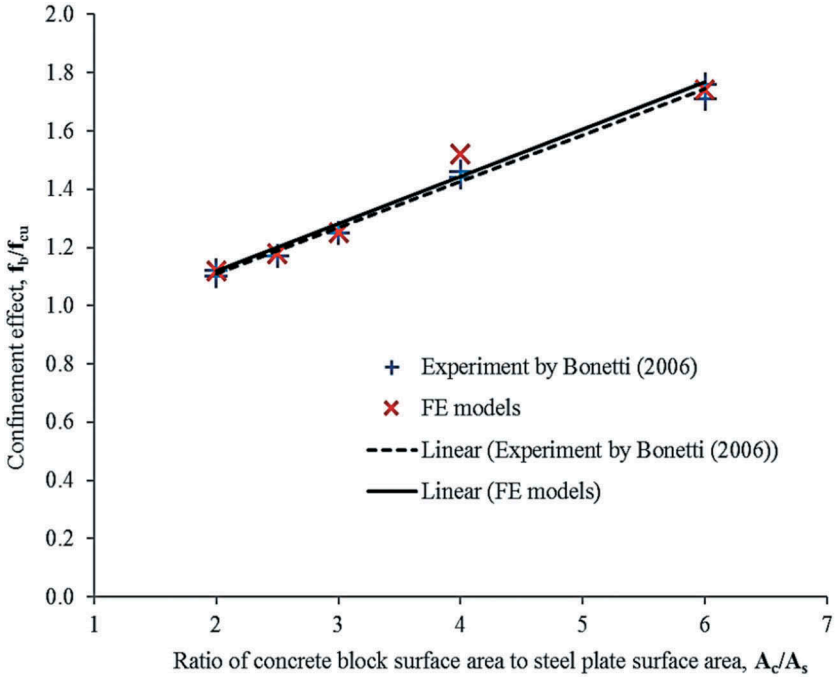

Figure 6. Comparisons of FE models with experiment results (Bonetti, 2005).

parameters to account for the difference in the compressive strengths used in the FE and experimental methods. The two dimensionless parameters are (1) the ratio of bearing pressure, f_b divided by the compressive strength of concrete, f_{cu} and (2) the ratio of concrete surface,A_c divided by surface area of steel bearing plate,A_s.

The FE results and the selected data for comparisons are presented in Table 3. It can be seen that the normalised results for both the experimental data and the FE models are consistent in term of confinement effects and the different is less than 5%. The trend in variation to confinement determined from both the experimental and the FE models is in good agreement as shown in Figure 6.

Figure 6 shows that the FE models capture the trend of confinement effect in different ratios of (A_c/A_s) similar to that the experimental work by Bonetti (2005). The confinement effect, f_b/f_{cu} from the FE models also well agreement with the experimental data for each ratio of (A_c/A_s). In order to ensure accuracy of the current model, the failure mode obtained from this model was compared with a real field problem of concrete spalling and edge cracking. Figure 8 shows the comparisons of failure modes obtained from the numerical modelling and the real failure case.

Figure 7 implies that stress singularity can cause localised damages such as concrete spalling due to combination of stress concentration and excessive bulging at the contact between steel bearing plate and concrete pedestals. It also illustrates that localised issue also leads to reduction of bearing area under the bottom bearing plate and shear cracking of the concrete pedestals. Figure 7(b) shows similar failure mechanism obtained from the numerical modelling as the critical tension failure zone is exhibited at the surrounding bearing area due to high tensile stresses and stress singularity at the sharp edge of the contact area. Figure 7(b)(ii) shows that the tension failure zone is located at the outer edge of the bearing area which explains the spalling concrete failure mechanism of the pedestal.

4. Results and discussion

The details of FE analysis results for this study are based on full scale model of 50 mm high unreinforced concrete pedestal with a compressive strength 32 MPa. For ease of explanation, certain key elements and critical nodes are identified whereby their FE results are discussed. As the prime aim of this present study is to understand the localised failure mechanisms in the concrete pedestal, the following four main structural responses are considered; (a) deformation shape, (b) load–displacement relationship, (c) stress concentration and (d) failure load.

4.1. Deformation shape

Structural response of concrete pedestal in term of deformation shape due to excessive plate penetration into the concrete surface is firstly investigated. The deformed shapes of the concrete pedestal are shown in Figure 8, in which 2D views of the deformed shapes of cut section are displayed. The dashed lines in these figures show the original shape. The load-displacement control causes the concrete surface at the contact area to have deformed downward (below broken red line) whereas the outer part of concrete edge to have

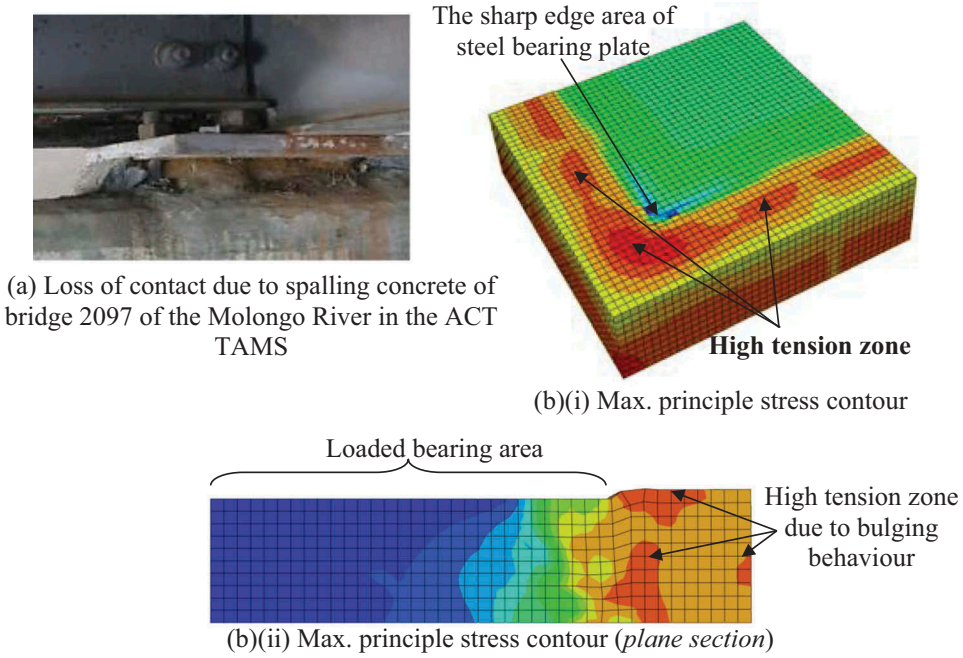

(a) Loss of contact due to spalling concrete of bridge 2097 of the Molongo River in the ACT TAMS

(b)(i) Max. principle stress contour

(b)(ii) Max. principle stress contour (*plane section*)

Figure 7. Failure modes: (a) observed in real photo; (b) obtained from numerical modelling.

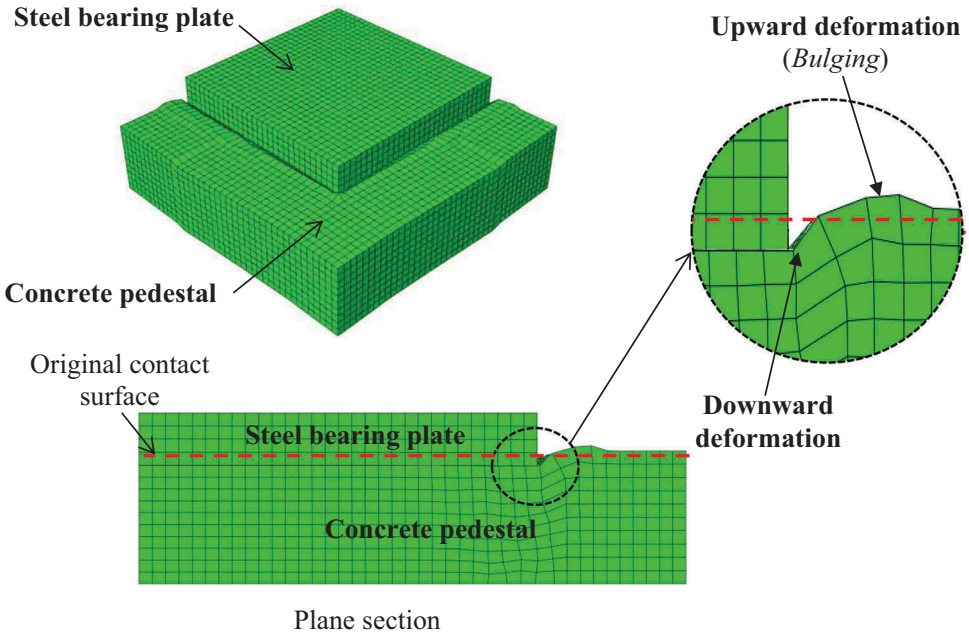

Figure 8. Deformation shape of concrete pedestal at ultimate load when vertical displacement reaches 0.114 mm (*100% of the ultimate load*).

deformed upward (above broken red line). Hence, the portion of concrete subject to downward deformation is under compression and upward deformation caused tension in concrete.

4.2. Load-applied displacement relationship

In order to provide load–displacement relationship of a concrete pedestal, the applied vertical load is taken as the summation of loads on all nodes on the top surface area of the steel plate. The load-applied displacement relationship obtained from the analysis is exhibited in Figure 9.

Figure 9 shows the load versus vertical displacement curve for the FE model. It can be seen that the ultimate load reaches up to 3668 kN which is only 2.86% higher than the predicted load of 3500 kN. The ultimate global failure load exhibited is at displacement of 0.114 mm (100% of the ultimate load). It is also notified that nonlinear behaviour of load distribution commences after the displacement reaches 0.022 mm about 30% of the ultimate load.

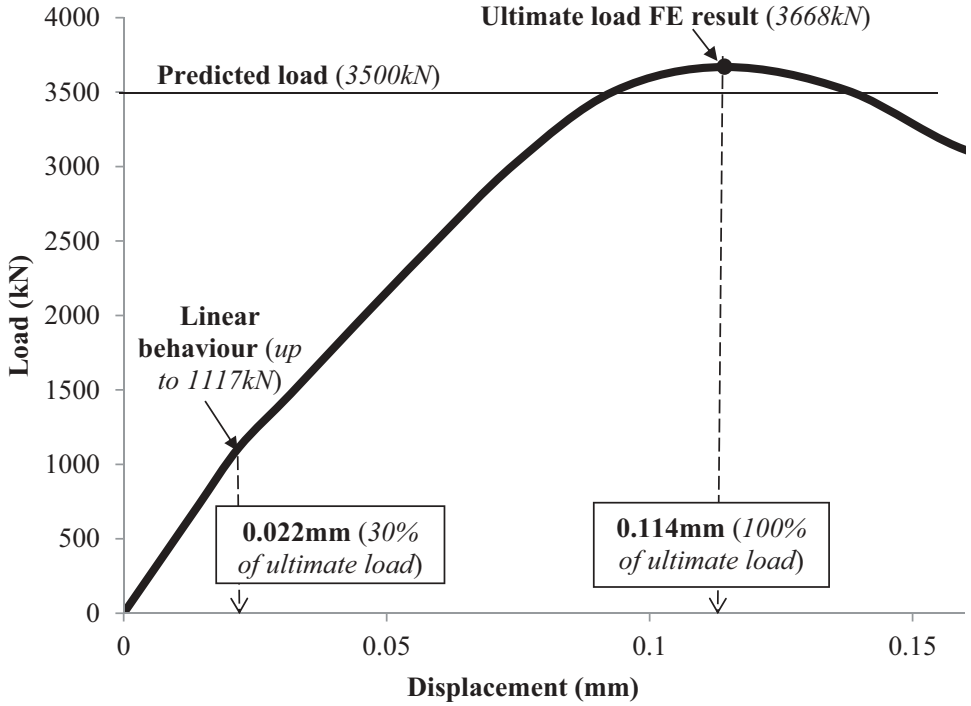

Figure 9. Load-applied displacement relationships.

4.3. Stress concentration

In the vertical stress distribution, it is observed that the stress levels are critical and localised at discontinuous regions especially near the sharp edge of contact area between the steel bearing plate and concrete surface. For comparison purpose, the stress contours are presented prior to and at ultimate load as vertical displacement reaches 0.022 mm (30% of the ultimate load) and 0.114 mm (100% of the ultimate load), respectively. The vertical stress contours prior to and at ultimate load are provided in Figures 10 and 11, respectively.

Figure 10 shows that the vertical stress in the compression zone just prior to the ultimate state was localised near the sharp edge of the concrete surface with a stress level of −29.09MPa. Even though the stress level of −29.09MPa in concrete is considered low, but it is critical as this value is close to compressive strength (32 MPa). It also can be noted that the outer edge of concrete surface exhibits tensile stress level of +1.68 MPa, which is the highest value for the concrete for 0.022 mm vertical displacement.

Figure 11 shows that when the load reaches ultimate, there is a significance change of maximum vertical

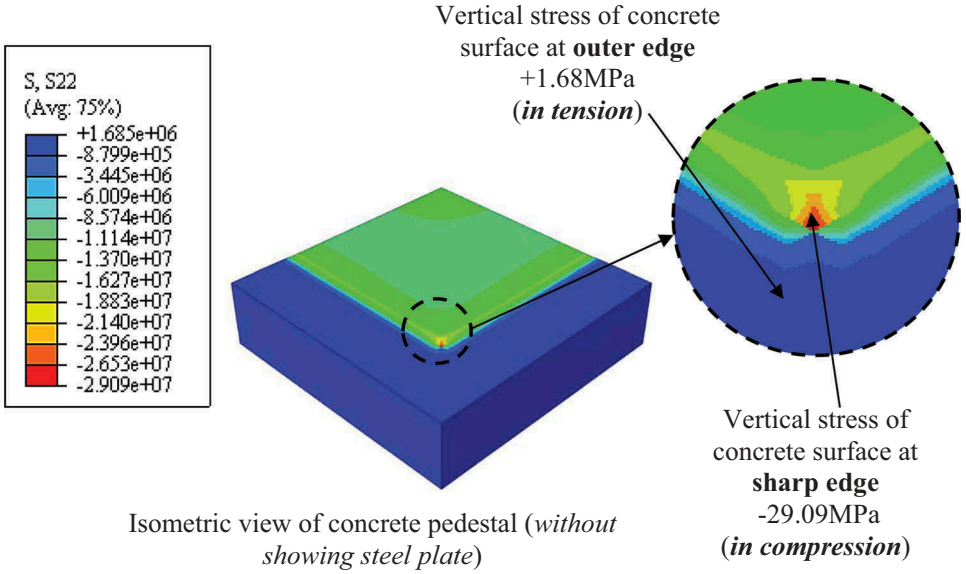

Figure 10. Vertical stress contour before ultimate load at concrete surface when the vertical displacement reaches 0.022 mm (*30% of the ultimate load*).

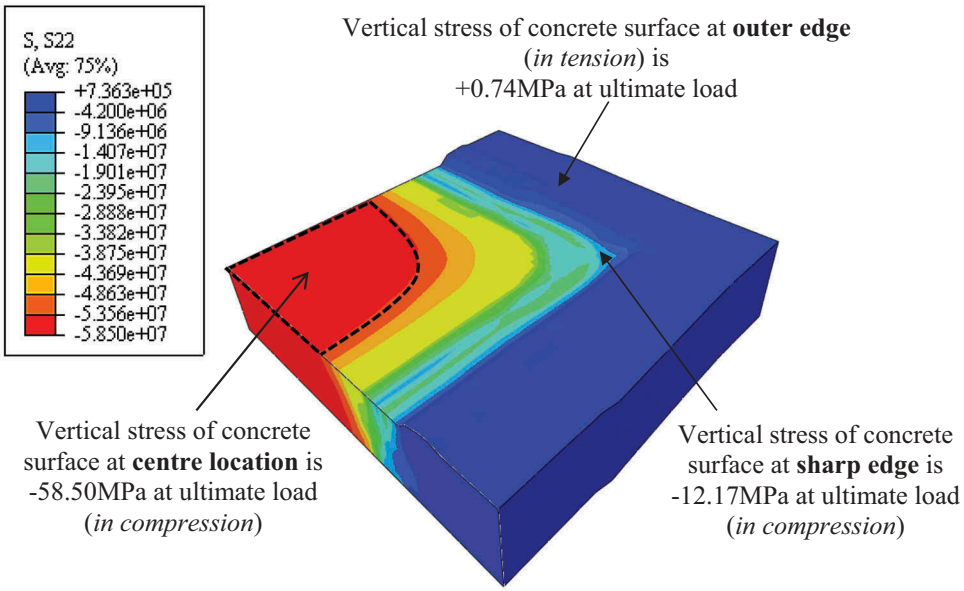

Figure 11. Vertical stress contour at failure when the vertical displacement reaches 0.114 mm (*100% of the ultimate load*).

compression stress contour pattern from uniform to different contour levels. The highest compression zone is concentrated at the area with comparatively high stress level of −58.50 MPa as compared to 29.09 MPa at the sharp edge prior to ultimate load (see Figure 10). The vertical stress contour zone gradually decreases towards the sharp edge down to −12.17 MPa. It is also notified that there is a significant stress reduction in tension zone at the outer edges of the concrete surface from +1.68 MPa (prior to ultimate load) to +0.74 MPa.

4.4. Failure load

Concrete pedestals severely suffer localised damage due to incompatible stiffness and discontinuities in the contact zone between the steel bearing plate and the concrete pedestals and high levels of stress concentration in the contact region. In order to explain localised damage, the failure load corresponding to localised failure was output. The ratio between the localised and global failure loads was calculated and presented. For the purpose of comparison, three key elements at different locations at different stress levels were selected. The three locations considered were (1) centre of pedestal, (2) mid-point between centre and sharp edge of contact area and (3) sharp edge at contact zone (see Figure 12). Figure 13 is plotted to compare the localised failure load caused by stress concentration corresponding to global failure load.

Figure 13 shows the localised failure load caused by stress concentration at sharp edge (1473 kN). This load is much lower than the global failure load of 3668 kN. The ratio of the localised-to-global failure load was predicted approximately as 0.4 by the FE model. The ultimate load predicted by the AASHTO LRFD (2014) and that of the Standard (2009), respectively, are 3330

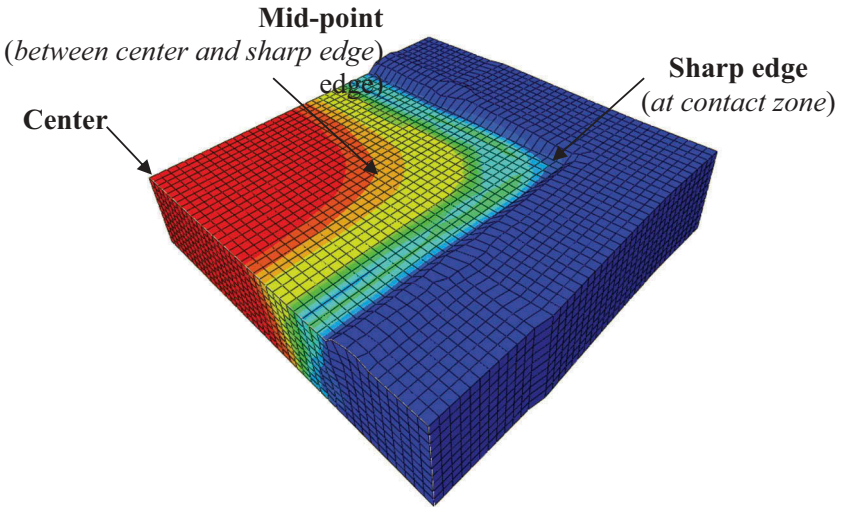

Figure 12. Three selected key elements for comparison purpose.

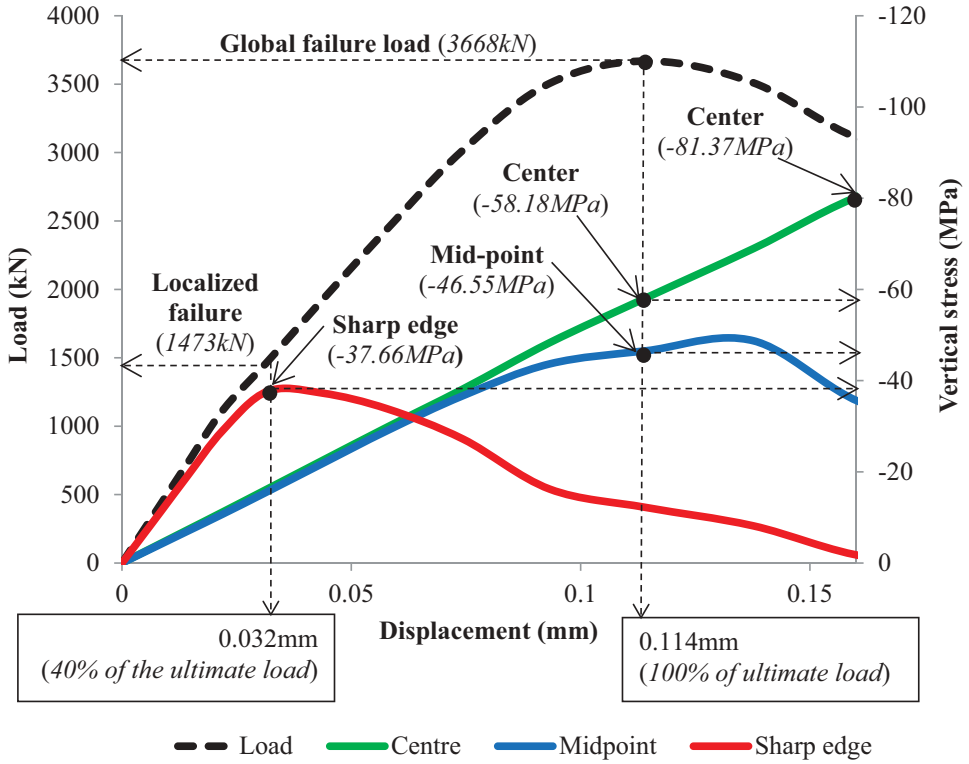

Figure 13. Localised failures in load-displacement at centre of pedestal, midpoint and sharp edge of contact zone.

and 3495 kN. This shows that the FE model is capable of predicting very close, but approximately 7% larger ultimate load than the standards.

The tensile stress corresponding to the localised failure stage in the FE model was 1.8 MPa as shown in Figure 14. It can also be observed that the maximum principle stresses of the elements at the middle of the edge and the centre of the pedestal are attained slightly later at displacement 0.044 mm (52% of ultimate load) and 0.058 mm (67% of ultimate load), respectively, compared to the stress at sharp edge. It clearly shows that the rate of increase of stress at sharp edge is faster than those at the mid-point and centre. The allowable tensile stress in the pedestals as per Standard (2009) is 2.28 MPa (using Eq. 6), which is 27% larger than the FE prediction, which shows that the Standard (2009) provision is not conservative. This provision, perhaps, has been guided by the expectation of confinement from bearing plates and the experimental data obtained from dog bone shaped tension specimens or Brazilian tests where cylinders are tested horizontally. Unfortunately, it appears the sharp edges are reducing the level of tensile cracking. Therefore, it is proposed to reduce the coefficient from 0.45 to 0.32 through simple calibration.

At the global failure load 3668 kN, it was noted that the element at the midpoint and centre location exhibited elastic behaviour with stress levels approaching −46.55 and −58.18 MPa, respectively – which is 43% and 81% greater than concrete strength, respectively. The increase in stress level in concrete beyond its compressive strength was possible due to the severe confinement the pedestal was subject to between the bearing plate and pier-head. It was also observed that the stress level at the midpoint increased up to −47.84 MPa. However, at the centre location it was more than −81.37 MPa even after the global failure load was realised. These increases were possible due to the confinement effect provided by the steel bearing plate placed on the concrete surface.

5. Conclusion

This paper presented an application of explicit FE method to explain the localised failure mechanism of concrete pedestals supporting the bridge girder bearings. The following conclusions have emerged from the analyses presented in the paper;

(1) The explicit FE model presented in this paper predicts the ultimate global failure load very close to the predictions of the AASHTO LRFD Bridge Design Specifications (2014) and Standard (2009).
(2) Localised failure of concrete pedestals supporting bridge bearings is shown to occur at 40% of the global failure load.
(3) It is recommended that the coefficient provided in Standard (2009) for allowable tensile stress in pedestals be reduced from 0.45 to 0.32 to avoid premature cracking and spalling of the concrete – especially close to the sharp edges and corners.

(4) The industry survey has also shown that spalling of concrete and edge cracking are the major types of localised failure in the concrete pedestals. Due to the technical difficulties, the industry prefers strategies to avoid premature failure of pedestals rather than improved maintenance strategies. The occurrence of the localised failure in pedestals might be linked to the higher allowable tensile stresses for the pedestals in Standard (2009).
(5) Localised damages occur near the sharp edge area due to stress concentration at the contact interface between the steel bearing plate and the concrete pedestal. Consequently, reduction of the bearing areas due to spalling concrete and edge cracking which could be translated into increase in damages and hence reduces in life of the pedestals.

Based on these conclusions, it is suggested that the premature failure of pedestals be eliminated through shaping of the sharp edges and corners of the pedestals and/or confining the pedestals laterally. The developed FE model is used to develop such strategies.

Acknowledgments

The authors acknowledge the financial support from Universiti Teknologi MARA (UiTM) Shah Alam, Selangor, Malaysia through BESTARI PERDANA research Grant 600-IRMI/Dana5/3/BESTARI (P) (060/2018) is greatly acknowledged. The authors also gratefully acknowledge support provided by Queensland University of Technology High Performance Computing (QUT-HPC).

Disclosure statement

No potential conflict of interest was reported by the authors.

Funding

This work was supported by the Universiti Teknologi MARA [600-IRMI/Dana5/3/BESTARI(P) (060/2018)].

Notes on contributors

M. Dhanasekar is a professor of infrastructure engineering at Queensland University of Technology, Brisbane, Australia. He is a chief investigator in the ARC Industrial Research Hub on road infrastructure and the ARC Industrial Training Centre on rail infrastructure. He is also an invited investigator in Project 'Dynamics of Railway Engineering' funded by the Government of China. Professor Dhanasekar has successfully supervised 16 PhD students in infrastructure engineering and 14 PhD students in general structural engineering. The chair of Professor Dhanasekar is partly funded by the Concrete Masonry Association of Australia. Professor Dhanasekar has published well over 200 peer-reviewed papers of which 60% of them are in high impact journals and secured approximately $4M research funds.

N. A. Yahya is currently a research coordinator at the Centre of Postgraduate Studies at Faculty of Civil Engineering at Universiti Teknologi MARA, Selangor, Malaysia.

H. Abd Hamid is a professor of civil engineering at Universiti Teknologi MARA, Selangor, Malaysia. Professor Abd Hamid has successfully supervised 10 PhD students in civil structural engineering. Professor Abd Hamid has published over 50 peer-reviewed papers.

ORCID

N. A. Yahya http://orcid.org/0000-0002-0558-0652

References

AASHTO LRFD Bridge Design Specifications. eds. 2014. American Association of State Highway and Transpo rtation Officials.

Abaqus User's Manual, eds. 2006. Incorporate.

ACI Committee 318. 1999. "Building Code Requirements for Structural Concrete (ACI 318-99) and Commentary (318R-99)." Farmington Hills, Mich.: America Concrete Institute, 391.

Ala, N., E. H. Power, and A. Azizinamini. 2016. "Experimental Evaluation of High-Performance Sliding Surfaces for Bridge Bearings." *Journal of Bridge Engineering* 21 (2).

Al-Rifaie, A., S. W. Jones., Q. Y. Wang, and Z. W. Guan. 2018. "Experimental and Numerical Study on Letral Impact Response of Concrete Filled Steel Tube Columns with End Plate Connections." *International Journal of Impact Engineering* 121: 20–34. doi:10.1016/j.ijimpeng.2018.07.003.

Austroads. 2012. "Design Rules for Bridge Bearings and Expansion Joints." *Austroads research report no. AP-R405 -12, report prepared by Hanson, N., I. Steele., and N. Lake Austroads Ltd.*, Sydney, New South Wales. ISBN: 9781921991264.

Bennett, M. 2014. "The Revision of AS5100. 4: Bearings and Deck Joints." Paper presented at the 9th Austroads Bridge Conference, October 22-24, in Sydney, New South Wales, Australia.

Bonetti, R., C. L. Roberts-Wollmann, and J. T. Santos. 2014. "Bearing Strength of Confined Concrete." *ACI Structural Journal* 111 (6): 1317. doi:10.14359/51687163.

Bonetti, R. A. 2005. "Ultimate Strength of the Local Zone in Load Transfer Tests." *Master diss.*, Virginia Polytechnic Institute and State University.

Chaudhari, S. V., and M. A. Chakrabarti. 2012. "Modeling of Concrete for Nonlinear Analysis Using Finite Element Code ABAQUS." *International Journal of Computer Applications* 44 (7): 14–18. doi:10.5120/6274-8437.

Dhanasekar, M., J. A. Thamboo, and S. Nazir. 2017. "On the In-plane Shear Response of the High Bond Strength Concrete Masonry." *Materials and Structures/Materiaux Et Constructions* 50 (5): 214.

Escobar-Sandoval, E. D., A. S. Whittaker, and G. F. Dargush. 2006. "Concentrically Loaded Circular Steel Plates Bearing on Plain Concrete." *Journal of Structural Engineering, ASCE* 132 (11): 1784–1792. doi:10.1061/(ASCE)0733-9445(2006)132:11(1784).

Freire, L. M., J. De Brito, and J. R. Correia. 2015. "Inspection Survey Of Support Bearings in Road Bridges." Journal of Performance of Constructed Facilities 29 (4).

Genikomsou, A. S., and M. A. Polak. 2015. "Finite Element Analysis of Punching Shear of Concrete Slabs Using Damaged Plasticity Model in ABAQUS." *Engineering Structures* 98: 38–48. doi:10.1016/j.engstruct.2015.04.016.

Hite, M. C., R. DesRoches, and R. T. Leon. 2008. "Full-scale Tests of Bridge Steel Pedestals." *Journal of Bridge Engineering* 13 (5): 483–491. doi:10.1061/(ASCE)1084-0702(2008)13:5(483).

Ince, R., and E. Arici. 2004. "Size Effect in Bearing Strength of Concrete Cubes." *Construction and Building Materials* 18 (8): 603–609. doi:10.1016/j.conbuildmat.2004.04.002.

Janaraj, T., and M. Dhanasekar. 2014. "Finite Element Analysis of the In-plane Shear Behaviour of Masonry Panels Confined with Reinforced Grouted Cores." *Construction and Building Materials* 65: 495–506. doi:10.1016/j.conbuildmat.2014.04.133.

Jankowiak, T., and T. Lodygowski. 2005. "Identification of Parameters of Concrete Damage Plasticity Constitutive Model." *Foundations of Civil and Environmental Engineering* 6 (1): 53–69.

Lee, J., and G. L. Fenves. 1998. "Plastic-damage Model for Cyclic Loading of Concrete Structures." *Journal of Engineering Mechanics* 124 (8): 892–900. doi:10.1061/(ASCE)0733-9399(1998)124:8(892).

Lubliner, J., J. Oliver., S. Oller., and E. Onate. 1989. "A Plastic-damage Model for Concrete." *International Journal of Solids and Structures* 25 (3): 299–326. doi:10.1016/0020-7683(89)90050-4.

Mishra, S. K., S. Gur, K. Roy, and S. Chakraborty. 2015. "Response of Bridges Isolated by Shape Memory–alloy Rubber Bearing." *Journal of Bridge Engineering* 21: 3.

Nguyen, H. H., and J. L. Tassoulas. 2009. "Directional Effects of Shear Combined with Compression on Bridge Elastomeric Bearings." *Journal of Bridge Engineering* 15 (1): 73–80. doi:10.1061/(ASCE)BE.1943-5592.0000034.

Noor-E-Khuda, S., M. Dhanasekar, and D. P. Thambiratnam. 2016. "An Explicit Finite Element Modelling Method for Masonry Walls under Out-of-plane Loading." *Engineering Structures* 113: 103–120. doi:10.1016/j.engstruct.2016.01.026.

Roberts-Wollmann, C. L., T. Banta, R. Bonetti, and F. Charney. 2006. "Bearing Strength of Lightweight Concrete." *ACI Materials Journal* 103 (6): 459–466.

Standard, A. 2009. *Concrete Structures AS3600-2009*. Sydney, New South Wales, Australia: Standards Australia Limited.

Starossek, U., N. Falah, and T. Lohning. 2010. "Numerical Analyses of the Force Transfer in Concrete-filled Steel Tube Columns." *Structural Engineering and Mechanics* 35 (2): 241–256. doi:10.12989/sem.2010.35.2.241.

Steelman, J. S. 2016. "Performance Of Nonseismic Ptfe Sliding Bearings When Subjected to Seismic Demands 1." *Journal Of Bridge Engineering* 21: 1.

Viljoen, H. S., A. A. Newmark, and B. E. Mawman. 1972. "Innovative Bearing Replacement Techniques for Black River Parkway Viaduct." *Civil Engineering = Siviele Ingenieurswese* 14 (10): 26–27.

Weisman, J., and G. P. Warn. 2011. "Stability of Elastomeric and Lead-rubber Seismic Isolation Bearings." *Journal of Structural Engineering* 138 (2): 215–223. doi:10.1061/(ASCE)ST.1943-541X.0000459.

Zahra, T., and M. Dhanasekar. 2016a. "Prediction Of Masonry Compressive Behaviour Using a Damage Mechanics Inspired Modelling Method." Construction and Building Materials 109: 128–138. doi:10.1016/j.conbuildmat.2016.01.048

Zhara, T. 2016b. "A Generalised Damage Model for Masonry under Compression." *International Journal Of Damage Mechanics* 25 (5): 629–660. doi:10.1177/1056789516656745.

Zong, N., and M. Dhanasekar. 2013a. "Minimization of Railhead Edge Stresses through Shape Optimization." *Engineering Optimization* 45 (9): 1043–1060. doi:10.1080/0305215X.2012.717075.

Zong, N., and M. Dhanasekar. 2013b. "Hybrid Genetic Algorithm for Elimination of Severe Stress Concentration in Railhead Ends." *Journal of Computing in Civil Engineering, ASCE* 29 (5).

Zong, N., and M. Dhanasekar. 2017. "Sleeper Embedded Insulated Rail Joints for Minimising the Number of Modes of Failure." *Engineering Failure Analysis* 76: 27–43. doi:10.1016/j.engfailanal.2017.02.001.